ELSEVIER

Engineering Analysis with Boundary Elements 28 (2004) 1111–1121

ENGINEERING ANALYSIS *with* BOUNDARY ELEMENTS

www.elsevier.com/locate/enganabound

A mixed BEM–FEM formulation for layered soil–superstructure interaction

Valério S. Almeida, João B. de Paiva*

Department of Structural Engineering, São Carlos School of Engineering, São Paulo University, Av. Trabalhador Sancarlense, 400, 13566-590 São Carlos, SP, Brazil

Received 1 April 2003; revised 17 March 2004; accepted 17 March 2004

Available online 12 May 2004

Abstract

The analysis of soil–structure interaction is a vast field of interest in the area of civil engineering. Any realistic representation of its behaviour is a complex numerical task owing to its extremely variable mechanical behaviour. In this paper a Boundary Element Method formulation (BEM) for the analysis of SSI is presented in which all dependent interactions (superstructure, infrastructure and the supporting soil) are considered. Thus, the soil is treated as an inhomogeneous continuum supported by a rigid and adhesive interface and modelled by BEM using the 3D Kelvin solution. The raft foundation and the superstructure are represented by finite shell and 3D frame elements. In order to estimate the accuracy and the potentiality of the proposed numerical formulation, some examples are validated by comparison with similar approaches, and other simulations are presented, to stress the need to analyse the inhomogeneous soil–raft-superstructure system as a whole.

Keywords: Boundary element method; Mixed boundary element method–finite element method formulation; Inhomogeneous soil; Flexible superstructure; Solution of sparse linear equations

1. Introduction

Soil–structure interaction (SSI) represents an integrated system. However, this complex problem is always analysed in separate parts. This simplification is generally necessary because of the intrinsic complexity of treating SSI as a whole, as each of the sub-systems, by itself, represents a vast field of possible mechanical idealizations and a wide choice of physical and geometrical parameters. Two different approaches to the problem are commonly found. One group of researchers is concerned with applying rigorous models to the superstructure and they usually consider the soil as a rigid base or use very simple models for the continuum. On the other hand, other authors are more interested in applying rigorous mechanical models to the soil without coupling it to the superstructure and/or they just consider a raft or a simple two-dimensional frame resting on the deformable soil.

However, several studies analyse SSI as an integrated system, but most of them simplify the problem by considering the structure in two-dimensional space [1,2] and the soil a homogeneous isotropic linear continuum in an infinite half-space, ignoring its highly heterogeneous and discontinuous nature [3–7].

Within the context of this integrated modelling strategy, much research effort has been dedicated over many decades to the modelling of the soil, considering it as an inhomogeneous continuum. One line of research models the heterogeneous media via analytical or semi-analytical formulations. The pioneering work of Burmister [8,9] discusses the technique of transforming integrals into partial differential equations (PDE), from which stress values are calculated for a given force applied on the surface of a two or three-stratum inhomogeneous medium. Poulos [10] integrated the solutions of Burmister for any type of loading, while Gibson [4] analysed the state of stress in an elastic inhomogeneous half-space, assuming a linear rise of stiffness with depth, for a given concentrated force on the surface. In addition, Chan et al. [11] generalised the solutions of Burmister for vertical and horizontal forces applied to the interior of two elastic strata forming the inhomogeneous half-space. Their solutions result from the use of the Fourier expansion of the Navier–Cauchy

* Corresponding author. Tel.: +55-16-273-9455; fax: +55-16-273-9481.
E-mail address: paiva@sc.usp.br (J.B. de Paiva).

0955-7997/$ - see front matter © 2004 Elsevier Ltd. All rights reserved.
doi:10.1016/j.enganabound.2004.03.002

equations. Hence, as in Burmister's work, the solutions are approximated to a series of exponential functions. Davies and Banerjee [12] repeated the approach used in Ref. [11], considering forces applied only at the boundary between strata.

Another line of research makes use of the powerful numerical methods for modelling heterogeneous media. Within this approach, two well-known methods are used on most occasions: Finite Element Method (FEM) and Boundary Element Method (BEM). Examples of FEM applied to SSI problems can be found in the literature [13–21], but this technique leads to a cumbersome procedure involving generating a mesh over the whole region, which makes FEM inappropriate for semi-infinite problems. In contrast, BEM is very well suited to the simulation of infinite elastic problems, because of its intrinsic formulation [22–25].

In one of the articles cited above [24], the technique known as *the method of successive stiffness* was applied, using Kelvin solutions to 2D problems. In this article, each layer of soil is treated as a homogeneous, isotropic and elastic region, to which equilibrium and compatibility conditions are applied.

The primary objective of the present paper is to expand the approach presented by Maier and Novati [24] to the analysis of a three-dimensional stratified half-space by BEM, taking into account the flexible superstructure by FEM, using shell elements and three-dimensional beam elements.

2. The boundary element method applied to problems in elastostatics

In the absence of volume forces, the Navier–Cauchy equations are given by:

$$u_{i,jj}(s) + \frac{1}{1-2\cdot\nu}\cdot u_{j,ji}(s) = 0, \qquad i,j = 1,2,3 \tag{1}$$

where $u_i(s)$ is the displacement in the orthogonal direction i from the point s inside the solid and satisfies certain boundary conditions, and ν is Poisson's ratio. These domain equations can further be expressed as surface equations, which are represented by the Somigliana Identity:

$$u_i(p) + \int_\Gamma p^*_{ij}(p,S)\cdot u_j(S)\partial\Gamma(S) = \int_\Gamma u^*_{ij}(p,S)\cdot p_j(S)\partial\Gamma(S) \tag{2}$$

where p and S are, respectively, the source point where a unit force is applied and a boundary point at the surface, u_j and p_j are, respectively, the real displacement field and surface forces on the boundary S in the jth direction, while u^*_{ij} and p^*_{ij} represent weighted field coefficients which indicate the response obtained in the direction j in S, to a force applied in the direction i at the point p. This identity is based on Betti's reciprocal theorem and weighted or fundamental solutions given by u^*_{ij} and p^*_{ij} represent particular solutions of the partial differential equations of Eq. (1) for a given boundary condition.

The strategy to obtain the boundary integral equations involves transferring p, which is inside the body, to the boundary. Thus, expression (2) can be written as follows:

$$C_{ij}(P)\cdot u_j(P) + \int_\Gamma p^*_{ij}(P,S)\cdot u_j(S)\cdot\partial\Gamma(S) = \int_\Gamma u^*_{ij}(P,S)\cdot p_j(S)\cdot\partial\Gamma(S) \tag{3}$$

where the integral in Eq. (3) is defined in the sense of the Cauchy principal value [26] and C_{ij} are coefficients that depend on the problem's geometry [27]. The fundamental solutions used herein are the known Kelvin solutions presented in Ref. [28] for the three-dimensional case.

Since the analytical solutions of expression (3) are not given in closed form, they have to be estimated numerically. Hence, the Boundary Element Method (BEM) is based on the assembly of a system of algebraic equations resulting from boundary integral equations, Eq. (3), written in terms of nodal variables that are approximated to the boundary values using shape functions. The integral equations of Eq. (3) are then written without considering the domain forces as:

$$C_{ij}(P)\cdot u_j(P) + \sum_{k=1}^{\mathrm{NE}} |J|\cdot\int_\Gamma p^*_{ij}(P,S)\cdot\Psi(S)\partial\xi(S)\cdot(U_i)^k = \sum_{k=1}^{\mathrm{NE}} |J|\cdot\int_\Gamma u^*_{ij}(P,S)\cdot\Psi(S)\partial\xi(S)\cdot(P_i)^k \tag{4}$$

where NE, ψ, J are, respectively, the number of boundary elements, the shape function and the Jacobian transformation. In this paper, all the surfaces of the soil layers were discretized into flat triangular elements [29] with linear shape functions of the form $\Psi_i(\xi_1,\xi_2,\xi_3) = \xi_i$, where ξ_i are homogeneous coordinates [29].

The integrals proposed in Ref. (4) cannot, however, be solved analytically for any generic surface; hence the use of numerical techniques such as those given in Refs. [30,31]. In the present paper, the integral equations are calculated numerically by using a three-dimensional triangular quadrature integral [29].

It is possible to assemble the shape matrices of Eq. (4), which takes on the following form:

$$[H]\cdot\{U\} = [G]\cdot\{P\} \tag{5}$$

where the Dirichlet and/or Neumann boundary conditions of the given problem are applied at each nodal point.

3. Analysis of layered soil by the *successive stiffness method*

Expression (5) is here extended to a homogeneous, isotropic and linear solid. Inhomogeneous problems can be solved by considering a combination of problems of

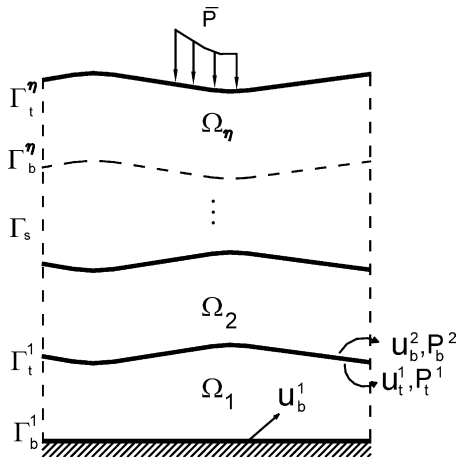

Fig. 1. Layered soil subjected to forces on the surface, base of boundary, top and side.

adjacent homogeneous domains, while applying the necessary equilibrium and compatibility conditions at the interfaces of the domains [26,29].

Consider a layered soil with η layers (Fig. 1). For any given layer i, it is possible to write the correlation between the influence matrices of Eq. (5) as:

$$[\,[H^i_t] \quad [H^i_b] \quad [H^i_s]\,]\cdot\begin{bmatrix} U^i_t \\ U^i_b \\ U^i_s \end{bmatrix} = [\,[G^i_t] \quad [G^i_b] \quad [G^i_s]\,]\cdot\begin{bmatrix} P^i_t \\ P^i_b \\ P^i_s \end{bmatrix} \tag{6}$$

where the subscripts t, b and s represent quantities pertaining to the upper (top), lower (bottom) and side boundaries and U and P are, respectively, nodal displacements and tractions of the top, bottom or side boundaries.

Expansion of Eq. (6) gives:

$$\begin{bmatrix} [H^i_{tt}] & [H^i_{tb}] & [H^i_{ts}] \\ [H^i_{bt}] & [H^i_{bb}] & [H^i_{bs}] \\ [H^i_{st}] & [H^i_{sb}] & [H^i_{ss}] \end{bmatrix}\cdot\begin{Bmatrix} U^i_t \\ U^i_b \\ U^i_s \end{Bmatrix} = \begin{bmatrix} [G^i_{tt}] & [G^i_{tb}] & [G^i_{ts}] \\ [G^i_{bt}] & [G^i_{bb}] & [G^i_{bs}] \\ [G^i_{st}] & [G^i_{sb}] & [G^i_{ss}] \end{bmatrix}\cdot\begin{Bmatrix} P^i_t \\ P^i_b \\ P^i_s \end{Bmatrix} \tag{7}$$

Equilibrium and compatibility conditions can then be imposed on displacements and stresses along the boundary between the ith and $(i+1)$th layers. For cases in which there are no relative movements between contact nodes, i.e. the case of ideal friction without the existence of prescribed forces at the interface and with an undisturbed side boundary, the conditions can be expressed as:

$$\{u^i_t\} = \{u^{i+1}_b\} \tag{8.1}$$

$$\{p^i_t\} = -\{p^{i+1}_b\} \tag{8.2}$$

$$\{u_s\} = \{0\} \tag{8.3}$$

$$\{p_s\} = \{0\} \tag{8.4}$$

with i varying from 1 to $\eta - 1$.

Assuming that the lateral surface is sufficiently remote, it is possible to adopt Eqs. (8.3) and (8.4) in Eq. (7) and thus obtain the influence matrix of each layer, which is given by:

$$\begin{Bmatrix} P^i_t \\ P^i_b \end{Bmatrix} = \begin{bmatrix} [K^i_{tt}] & [K^i_{tb}] \\ [K^i_{bt}] & [K^i_{bb}] \end{bmatrix}\cdot\begin{Bmatrix} U^i_t \\ U^i_b \end{Bmatrix} \tag{9}$$

Hence, applying Eq. (9) to each layer i, and invoking Eqs. (8.1) and (8.2), this layer can easily be related to its neighbours.

In the lowest layer $i = 1$, the displacement at this base is null, giving a fixed medium and for which expression (9) can be re-written as:

$$\{P^1_t\} = [K^1_{tt}]\cdot\{U^1_t\} \tag{10}$$

$$\{P^1_b\} = [K^1_{bt}]\cdot\{U^1_t\} \tag{11}$$

For $i = 2$, one has, from expression (9):

$$\{P^2_t\} = [K^2_{tt}]\cdot\{U^2_t\} + [K^2_{tb}]\cdot\{U^2_b\} \tag{12}$$

$$\{P^2_b\} = [K^2_{bt}]\cdot\{U^2_t\} + [K^2_{bb}]\cdot\{U^2_b\} \tag{13}$$

After applying the conditions Eqs. (8.1), (8.2) and (10) to Eq. (13), we have:

$$\{U^2_b\} = -[(K^1_{tt} + K^2_{bb})^{-1}\cdot K^2_{bt}]\cdot\{U^2_t\} \tag{14}$$

and substitution of Eq. (14) in Eq. (12) gives:

$$\{P^2_t\} = [[K^2_{tt}] - [K^2_{tb}]\cdot([K^1_{tt}] + [K^2_{bb}])^{-1}\cdot[K^2_{bt}]]\cdot\{U^2_t\} \tag{15}$$

which may be written:

$$\{P^2_t\} = [\hat{K}^2]\cdot\{U^2_t\} \tag{16}$$

The above equation represents the influence of layers 1 and 2. Hence, applying Eqs. (9), (8.1) and (8.2) to the layers i and $i+1$, we have:

$$\{P^i_t\} = \lfloor[K^i_{tt}] - [K^i_{tb}]\cdot([\hat{K}^{i-1}] + [K^i_{bb}])^{-1}\cdot[K^i_{bt}]\rfloor\cdot\{U^i_t\} \tag{17}$$

Thus, for the topmost layer $i = \eta$ and:

$$\{P^\eta_t\} = [\hat{K}^\eta]\cdot\{U^\eta_t\} \tag{18}$$

where P^η_t and U^η_t are the nodal parameters at the soil surface.

At this point, the influence of the inhomogeneous soil is entirely expressed by Eq. (18), which can be solved directly by applying the given loading conditions on the surface or by coupling the superstructure, using FEM or BEM.

4. Superstructure composed of laminar elements

To simulate the raft via the FEM, we superpose two independent formulations, one to represent the membrane

effect and the other the plate effect. The finite element adopted is thus a combination of the triangular membrane element, with a rotational degree of freedom, called Free Formulation, according to Bergan and Felippa [32], and the triangular plate element called Discrete Kirchhoff Theory (DKT) described by Batoz [33]. This flat shell element is formulated by generating a stiffness matrix for a plane triangle in a three-dimensional space. The resulting combined plate-membrane system is represented by:

$$K_{(\mathrm{FF+DKT})} \cdot u^{\mathrm{nodal}}_{(\mathrm{FF+DKT})} = F_{(\mathrm{FF+DKT})} \tag{19}$$

where the displacement parameters of element e with nodes i, j and k at the vertices are expressed by:

$$\{u_{\mathrm{e}}\}^{\mathrm{T}} = \{(u \quad v \quad \theta_{x_3} \quad w \quad \theta_{x_1} \quad \theta_{x_2})_i (\,.\,.)_j (\,.\,.)_k\} \tag{20}$$

where u, v and w are the displacements and θ_{x_1}, θ_{x_2} and θ_{x_3} are the rotations obtained in the directions 1, 2 and 3, respectively, at each vertex node.

5. Superstructure composed of 3D buildings subjected to vertical and horizontal forces

The buildings are modeled with three-dimensional finite bar elements representing the linear elements of beams and columns, without considering the effect of torsion on them. The slabs in the buildings are considered as diaphragms with infinitely stiff horizontal planes, for which reason the horizontal displacements on each floor (u, v and θ_{x_3}) are the same. Therefore, all the influences of the columns and beams on each floor are transferred to a single master node, which is at the torsion centre. This building model considerably reduces the number of degrees of freedom of the final system.

The vertical forces are applied to the beams, either pointwise or distributed, while the horizontal and torsional forces, caused by the effect of wind should be applied pointwise at the center of torsion for each floor.

On the ground, the columns are coupled to the shell elements of the raft, forming a stiffness matrix that contains the influence of the raft-building set. The influence of the soil must then be coupled to this system, so that the soil–raft-building system can be analysed.

6. BEM–FEM coupling

Many techniques are used to combine the boundary and FEMs. However, these may be collected, for simplicity, into two approaches: (i) treating the boundary element as a part of the finite element region and (ii) treating the finite element as equivalent to a boundary element region. Both algebraic approaches are clearly presented in Ref. [29]. To apply the BEM–FEM coupling using the *successive stiffness method* to represent the soil and the conventional FEM, formulated in Sections 4 and 5, to handle the superstructure, it is reasonable to use the first approach (*i*), because the inversion of the non-banded G matrix has already been performed in the intrinsic formulation.

Briefly, the BEM–FEM coupling technique applied here consists in representing the forces at the soil surface given in Eq. (18), as nodal reactions between the contact elements across the superstructure-soil interface. Provided the reactions of the raft are expressed as forces already integrated into the domain and transformed into equivalent nodal forces in each BEM element, the surface forces of the soil can be expressed by nodal parameters distributed in the element. Hence, coupling requires transforming the surface forces into equivalent concentrated forces. This approach is presented below and more details can be seen in Ref. [29].

The approach described so far will be applied to the case of transverse loading, although it can be extended to the other two directions. Fig. 2 shows the transverse surface forces and the equivalent nodal forces.

In Fig. 2, g_i, g_j and g_k represent the surface forces at vertices i, j and k of a generic element, while F_i, F_j and F_k represent the equivalent nodal forces at the respective nodes.The work due to the external load in the element's transverse direction can be expressed as:

$$T_{\mathrm{e}} = \int_A g(x_1, x_2) \cdot w(x_1, x_2) \mathrm{d}A \tag{21}$$

where $w(x_1, x_2)$ and A are, respectively, the transverse displacement field within the element domain and the area of the element. When the variation of the displacement field is assumed to be linear:

$$w = w_i \xi_1 + w_j \xi_2 + w_k \xi_3 \tag{22}$$

Similarly, the surface forces can be expressed as:

$$g = g_i \xi_1 + g_j \xi_2 + g_k \xi_3 \tag{23}$$

After transforming the Cartesian coordinates into homogeneous coordinates [34] and substituting the expressions for g and w into Eq. (21), we have:

$$T_{\mathrm{e}} = \int_A (g_i \xi_1 + g_j \xi_2 + g_k \xi_3) \cdot (w_i \xi_1 + w_j \xi_2 + w_k \xi_3) \mathrm{d}A \tag{24}$$

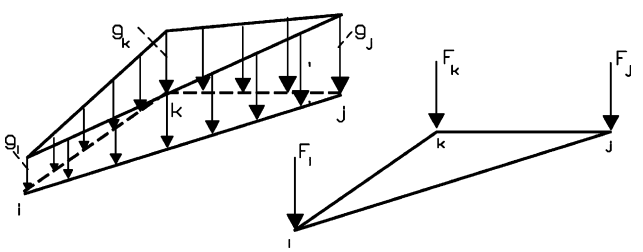

Fig. 2. Equivalent surface and nodal forces.

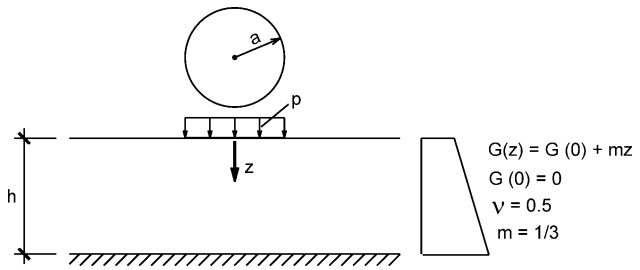

Fig. 3. Finite stratum under uniform circular loading.

Table 1
Percentage error of the central surface displacement

Thickness factor *h/a*	Layers	Error (%)
2	2	13.36
2	3	2.20
2	5	1.54
8	3	52.96
8	7	19.44
8	20	0.71

Moreover, minimising the portion of potential energy due to external loading and keeping in mind that the integral $\int_A f(\xi_1,\xi_2,\xi_3)\mathrm{d}A$ can be determined by:

$$\int_A \xi_1^{\eta_1}\xi_2^{\eta_2}\xi_3^{\eta_3}\,\mathrm{d}A = 2A\frac{\eta_1!\eta_2!\eta_3!}{(\eta_1+\eta_2+\eta_3+2)!} \tag{25}$$

the transverse nodal force vector is then given by:

$$\begin{Bmatrix} F_i \\ F_j \\ F_k \end{Bmatrix} = \frac{A}{12}\cdot\begin{bmatrix} 2 & 1 & 1 \\ 1 & 2 & 1 \\ 1 & 1 & 2 \end{bmatrix}\cdot\begin{Bmatrix} g_i \\ g_j \\ g_k \end{Bmatrix} \tag{26}$$

By following the same procedure in the other directions, the relation between the nodal and surface forces for the case of the Free Formulation and DKT element can be written as:

$$\begin{Bmatrix} F_i^{\ell} \\ F_j^{\ell} \\ F_k^{\ell} \end{Bmatrix} = [\bar{Q}]\cdot\begin{Bmatrix} g_i^{\ell} \\ g_j^{\ell} \\ g_k^{\ell} \end{Bmatrix} \tag{27}$$

where $\ell = 1,2,3$ represent the three orthogonal directions of the element and the matrix $\bar{Q}$ is given by:

$$[\bar{Q}] = \frac{A}{12}\cdot\begin{bmatrix} 2 & 1 & 1 \\ 1 & 2 & 1 \\ 1 & 1 & 2 \end{bmatrix} \tag{28}$$

Summing the contributions of all the finite elements and then minimising the energy functional, gives:

$$[K_{\mathrm{fem}}]\cdot\{U_{\mathrm{fem}}\} = \{F_{\mathrm{fem}}\} - [\bar{\bar{Q}}]\cdot\{P_r\} \tag{29}$$

where $U_{\mathrm{fem}}, F_{\mathrm{fem}}, P_r, K_{\mathrm{fem}}$ and $\bar{\bar{Q}}$ are, respectively, the vector of superstructure displacements, the vector of equivalent nodal forces due to external loading, the expanded vector of surface force due to soil reaction, the global stiffness matrix of the shell structure and the expanded transformation matrix resulting from the contribution of all the boundary elements.

Hence, by substituting Eq. (20) into Eq. (18) and applying equilibrium and compatibility conditions between the contact surfaces, we obtain:

$$[K_{\mathrm{fem}}]\cdot\{U_{\mathrm{fem}}\} = \{F_{\mathrm{fem}}\} - [\bar{\bar{Q}}]\cdot[\widehat{K}^{\eta}]\cdot\{U_{\mathrm{t}}^{\eta}\} \tag{30}$$

Eq. (30) can be simplified here, resulting in:

$$[K_{\mathrm{bem/fem}}]\cdot\{U_{\mathrm{bem/fem}}\} = \{F_{\mathrm{bem/fem}}\} \tag{31}$$

with:

$$[K_{\mathrm{bem/fem}}] = [K_{\mathrm{fem}}] + [\overline{\overline{Q}}]\cdot[\hat{K}^{\eta}] \tag{32}$$

7. Numerical examples

The ad hoc algorithm developed herein allows for both the independent analysis of the inhomogeneous soil and the analysis of the soil–raft-superstructure as a whole.

7.1. Finite layer with linear variation of modulus

This example presents an analysis of the soil, treated an inhomogeneous, linear isotropic medium. For the specific case of an uniformly distributed load applied to a circular region on the soil surface, the governing law for the stiffness

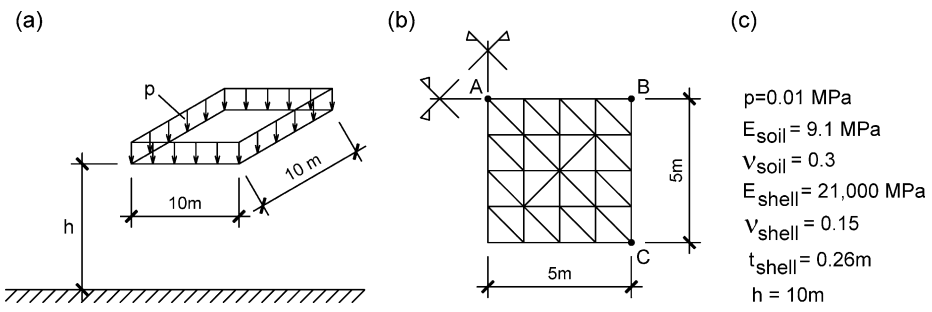

Fig. 4. (a) Thick plate on a non-deformable base; (b) discretization of a quarter of the plate; (c) Physical and geometric parameters of soil and shell.

Table 2
Results for some points on the thin plate

Point of plate	Fraser and Wardle [35]	Kolaî and Nemec [38]	Sadecka [36]	Present work
A [Deflections $w \times 10^{-3}$ (m)]	7.30	5.36	6.18	6.47
B [Deflections $w \times 10^{-3}$ (m)]	4.50	4.73	3.97	4.62
C [Deflections $w \times 10^{-3}$ (m)]	2.80	3.76	2.25	2.95
A [Moments M_{11} (kN/m^2)]	6.20	3.09	6.58	6.22

modulus is considered to follow a linear increase with depth (see Fig. 3). The results given in Table 1 demonstrate the formulation's consistency, even when the relation *h*/*a* is varied, and the inclusion of additional layers as this index (*h*/*a*) increases is necessary in order to represent better the linear variation of the soil's rigidity. The relative errors of the central surface displacement are obtained by comparing the values found by this formulation with those calculated by the semi-analytical expression of Burmister in Refs. [8,9].

7.2. Thin plate on a non-deformable base

In this case, the displacement and bending moment response in a thin square plate in contact with soil is estimated. The rigid base plane is located 10 m below the surface. Fig. 4 illustrates the discretisation, and the physical and geometric characteristics of the soil.

The results of this formulation are compared with other studies, showing a strong congruence with the values found by Fraser and Wardle [35] and Sadecka [36] as it can be seen in Table 2. The first authors [35] model the semi-infinite, using surface elements [37], in which the matrix is obtained using integral transform techniques, and Sadecka [36] calculates the displacements along the depth of the soil strata defined by non-linear weight functions, introducing the influence of the thin plate supported on the free surface of the soil and using FEM.

7.3. Loading on a square area with a rough rigid base

In this example, the soil surface is subjected to an external load distributed over a square area (see Fig. 5). The resulting displacements calculated by the present method, the approximate Steinbrenner method and the Burmister models [8,9] for the elastic medium are listed in Table 3 for several depths of the rigid base. For the region of the discretized surface we used a mesh with 748 nodes, of which 441 nodes (800 elements) were allocated to the central area of the loaded square and 307 nodes (518 elements) to the load-free area. The modulus of elasticity adopted for the soil was 100 MPa and its Poisson's ratio was 0.3.

Table 3 shows good agreement between the values obtained with this formulation and the semi-analytical model of Burmister [8,9]. As Poulos [10] indicates, Steinbrenner's simple approximate method underestimates the displacement values and, as the undeformable layer approaches the soil surface, these values are 10–15% lower. On the other hand, with the formulation presented here, this variation does not influence the results, which show an error of less than 1%.

Table 4 illustrates the robustness of the present formulation when it is applied to different numbers of layers representing the stratified homogeneous medium. The present approach is compared with the well-known Mindlin's formulation [39] for the elastic half-space and there is good agreement between the two, even when several layers are used to simulate the homogeneous half-space.

7.4. Multi-storey building on raft foundation supported on an inhomogeneous soil

The purpose of this example is to check the effect of both the variation of the soil's properties with depth and the position of the undeformable layer on a multi-storey building supported on a raft foundation.

The strains and forces acting on the beams, columns and raft foundation, as well as the soil's reaction forces, are

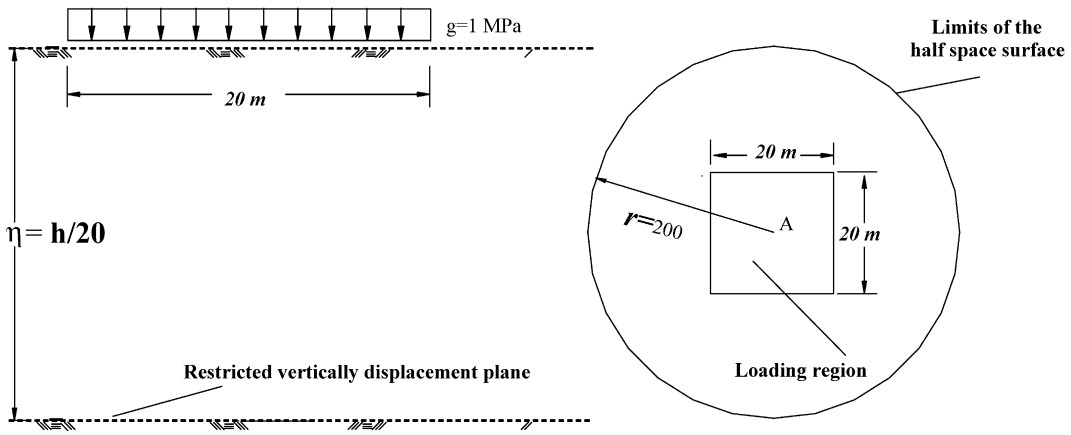

Fig. 5. Finite stratum under uniform loading.

Table 3
Vertical displacement (m) of point A

$\eta = h/L$	Burmister [8,9]	Present work (% error)	Steinbrenner (% error)
1	0.1290	0.1299 (0.7)	0.1171 (9.2)
2	0.1639	0.1650 (0.7)	0.1564 (4.6)
5	0.1876	0.1883 (0.4)	0.1845 (1.7)
50	0.2026	0.2037 (0.5)	0.2022 (0.2)

Table 4
Vertical displacement (m) of point A for different layers

$\eta = h/L$	Present work (layers)	% Error $[100(w - w_{exact})/w_{exact}]$
50	0.2037 (1)	−0.24
50	0.2037 (2)	−0.28
50	0.2036 (5)	−0.33
100	0.2041 (1)	−0.06
200	0.2042 (1)	−0.02
$w_{exact} = 0.2042$ (Mindlin's formulation)		

based on a 12-storey residential building plan whose permanent forces are stipulated in the Brazilian Code NBR 6118 [40] and variable wind forces specified in the Brazilian Code NBR-6123 [41]. The same mesh of elements as those of the previous example 7.3 is used, except that, in the area where loading is applied, the shell structure is now coupled and the building loaded onto it.

Fig. 6 illustrates the plans of the analysed structure, the tables of the geometry and the forces considered to act on each structural element of the multi-storey building. The raft self-weight load was neglected in the analysis. Fig. 7 shows the calculated transverse displacements (w) along the raft's AA cut, considering the soil–raft-building interaction for four cases (see Fig. 6a).

Note that taking into account the soil's rigidity throughout its depth results in a significant alteration in the displacement values of the soil–raft-building system, since the relative differences between cases b and c is about 90% (see Fig. 7). This influence proves to be more relevant than that of the position of the indeformable layer, since

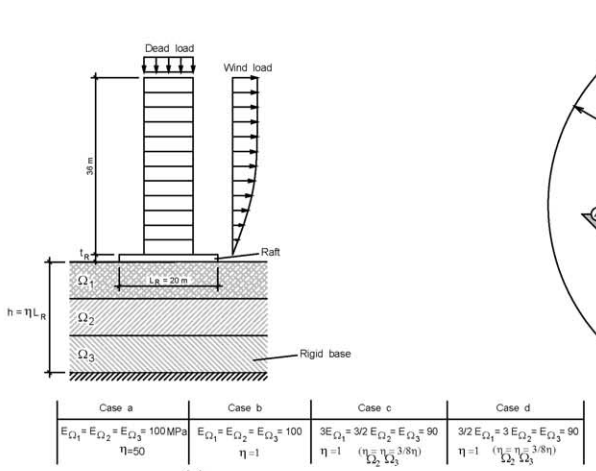

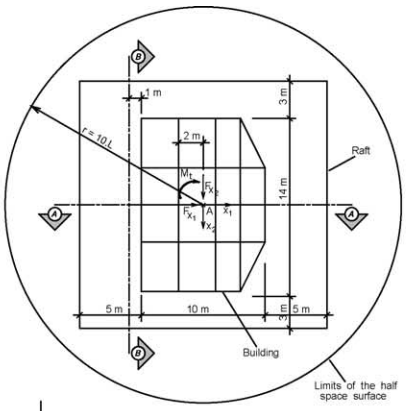

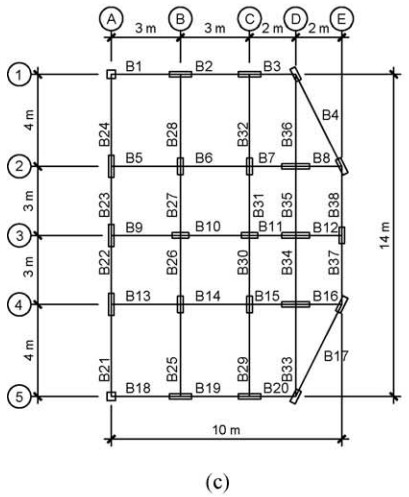

DEAD LOADING (kN/m)		
Floor Loading	**Roof Loading**	**BEAMS**
4.5	3.0	B1,B18,B22,B23
3.75	2.5	B2,B19
3.0	2.0	B3,B20
0.67	0.45	B4,B17
9.0	6.0	B5,B7,B9,B13,B15 B26,B27,B30,B31
9.75	6.5	B6,B14,B29,B32
8.5	5.67	B34,B35
6.0	4.0	B8,B12,B16
12.0	8.0	B10,B11
5.63	3.75	B21,B24
10.78	7.12	B25,B28
8.25	5.5	B33,B36
4.0	2.67	B37,B38

TYPE	COLUMNS (m^2)	BEAMS (m^2)
1	0.4x0.4	0.2x0.4
2	0.2x0.6	0.2x0.3
3	0.2x0.8	-
4	0.2x1.2	-
5	0.2x0.4	-

(d)

WIND LOADING			
Floor	F_{x_1} (kN)	F_{x_2} (kN)	M_t (kN m)
1	43.92	32.80	13.89
2	50.43	37.64	15.95
3	53.86	40.20	17.04
4	55.82	41.67	17.66
5	56.89	42.46	18.00
6	57.35	42.81	18.14
7	57.36	42.82	18.15
8	57.04	42.58	18.04
9	56.45	42.14	17.86
10	55.65	41.54	17.61
11	54.68	40.82	17.30
12	53.57	39.98	16.95

COLUMNS	BEAMS	TYPE
A1,A5	All of the others	1
B1,C1,E3,B5,C5	B1→B4 ; B17→B20	2
A2,B2,C2,A3,B3,C3,A4,B4,C4	-	3
D2,D3,D4	-	4
D1,E2,E4,D5	-	5

Fig. 6. (a) Configuration of the structural scheme and the cases considered. (b) Schematic plan of the raft-building model. (c) Floor plan of the building. (d) Tables of the forces and dimensions of the building's linear elements.

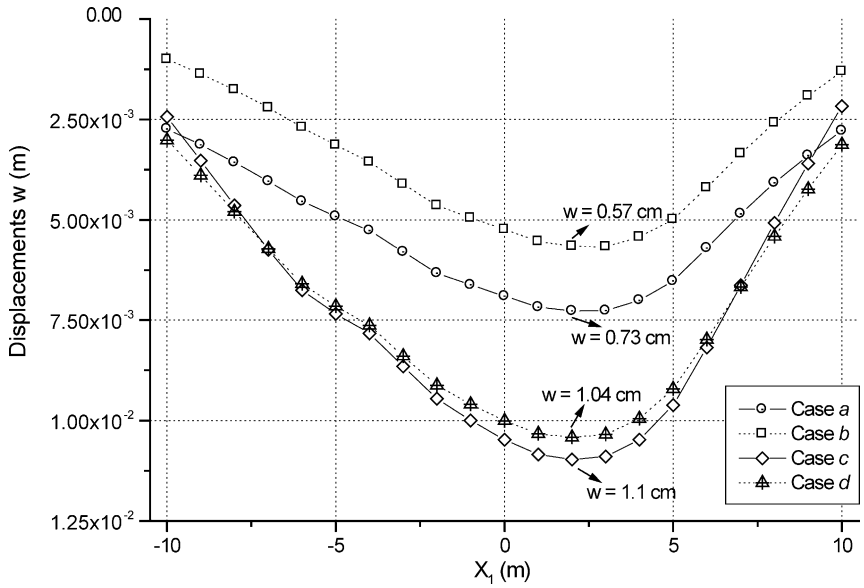

Fig. 7. Vertical displacements along section AA.

the relative difference in displacements between cases a and b is in the order of 30%.

Fig. 8 shows the distribution of bending moments M_{x_2} on the raft for case b. The critical values are located in the contact between column and raft, and the maximum value obtained is about 0.20 MNm/m in column D4. The negative values indicate that the inferior fibers of the raft are tensioned.

Fig. 9 shows the values of the stresses (σ_{33}) mobilized over the whole area of contact between soil and raft. The contact stress distribution is similar to that of bending moments, and the traction values obtained are around 0.06 MPa in case b.

Horizontal and vertical displacements at each storey along column C3 are depicted in Fig. 10, and comparisons between these displacements for case b and the rigid base are presented. The biggest difference occurs in vertical deflections where for case b the values are about three times those found for the rigid base.

Fig. 11 depicts bending moment distribution on column A3 and beam B9 storeys 2 and 3, for the building resting on undeformable soil and case c. The difference in moment between the two cases is particularly pronounced for dead loading, where the values for case c are around 100% greater than for undeformable soil case.

Table 5 presents the normal force that occurs in four columns, viz. a corner column A1, an edge column B1 and two central columns B2–B3. The results

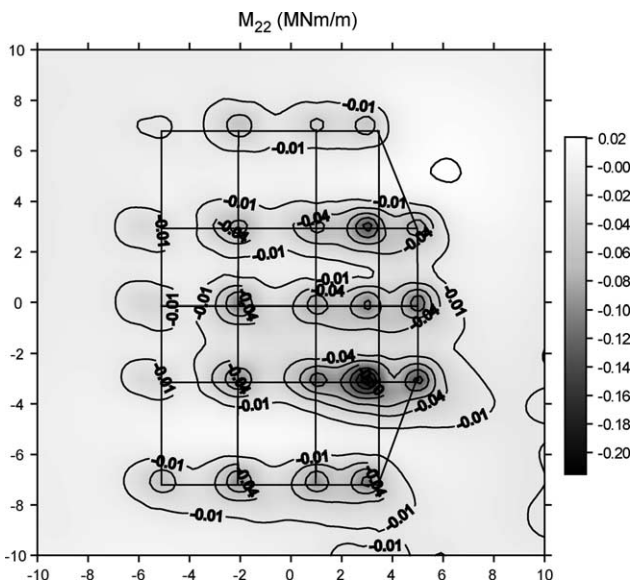

Fig. 8. Bending moments M_2 between soil and raft for the case b.

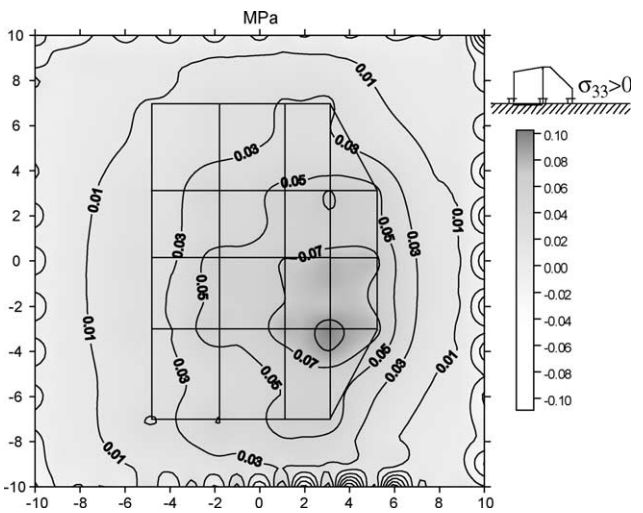

Fig. 9. Contact forces between soil and raft for the case b.

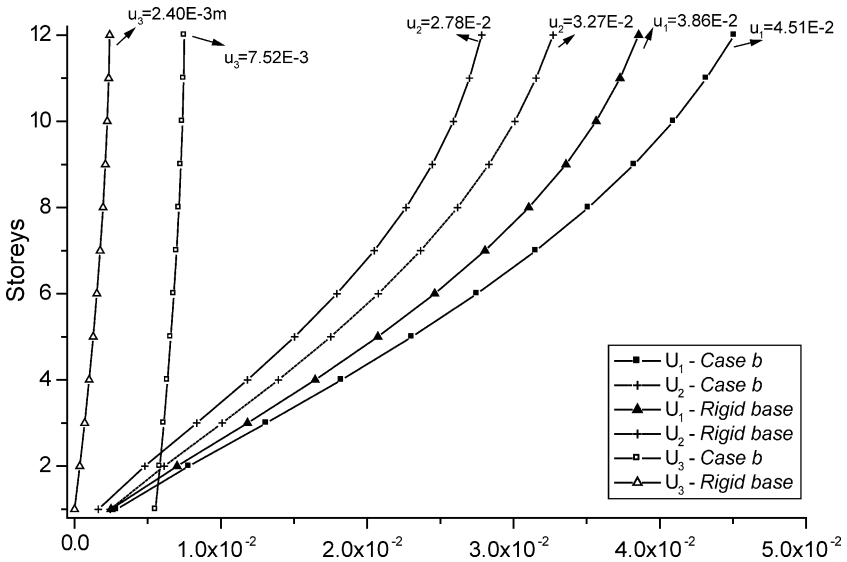

Fig. 10. Horizontal and vertical displacements across the storeys (column C3).

give an indication that the columns' normal values are closely distributed around the average, i.e. there is a more uniform redistribution of forces because the mobilisation of the soil–raft-building system occurs simultaneously.

In the solution of the linear system generated by coupling the soil-shell-multi-storey building—as in the present example—the resulting matrix is not symmetric, but sparse, with 26% nonzero elements (see Fig. 12). Thus, it is imperative to use sparse techniques for the solution of the problem. In the present research three different methods of solving the final linear equations were used: (i) the Fortran 90 code that uses IMSL routines [42]; (ii) the iterative method GMRES [43] optimized with a diagonal preconditioning (Jacobi); and (iii) the Harwell sparse matrix package MA28 [44].

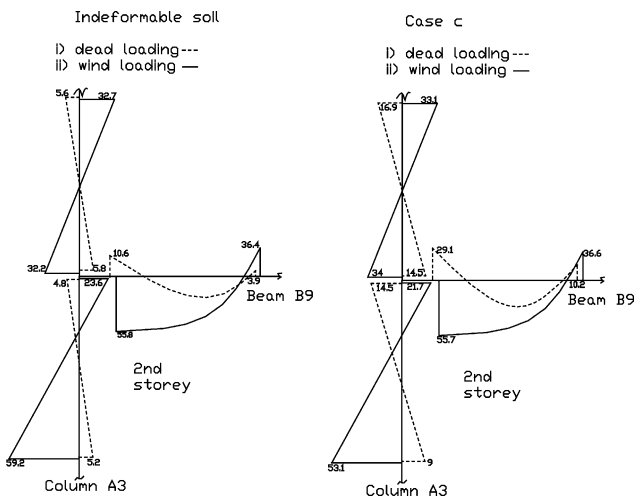

Fig. 11. Bending moments (kNm) between storeys 2 and 3.

The first, which is based on the direct method does not take into account the sparse pattern property of the final matrix, so it is not appropriate for this problem, as can be verified from the execution time in Table 6.

The second is the most conventional iterative method applied in solving sparse unsymmetric linear systems. The computational cost of the method is the matrix-vector product carried out at each iteration, and the sparse pattern generated in the final matrix is not a relevant factor for the convergence in the method. But the performance dependence of GMRES [43] strongly dependent on the condition number of the matrix, and the application of BEM in elastostatic problems, in general, does not generate a well-conditioned matrix property, principally in the zone and BEM–FEM coupling methods.

In the Harwell sparse matrix package MA28 [44], based on Gauss elimination, the data structure of the matrix is a determinant factor for rapid execution of code, due essentially to the fill-in effect. However, the sparse pattern generator software was not used to reduce the number of operations. Despite this, the execution time obtained with MA28 [44] showed it to be highly efficient in solving problems based on the mixed BEM–FEM formulation.

Table 5
Nominal forces (MN) in the columns of the ground floor for the several cases of soil rigidity

Column	Case a	Case b	Case c	Case d	Indeformable soil
A1	0.0687	0.0661	0.1139	0.0896	0.0359
B1	0.3021	0.3024	0.3222	0.3694	0.2875
B2	0.4670	0.4666	0.4330	0.4457	0.5153
B3	0.5477	0.5449	0.5116	0.5142	0.6205

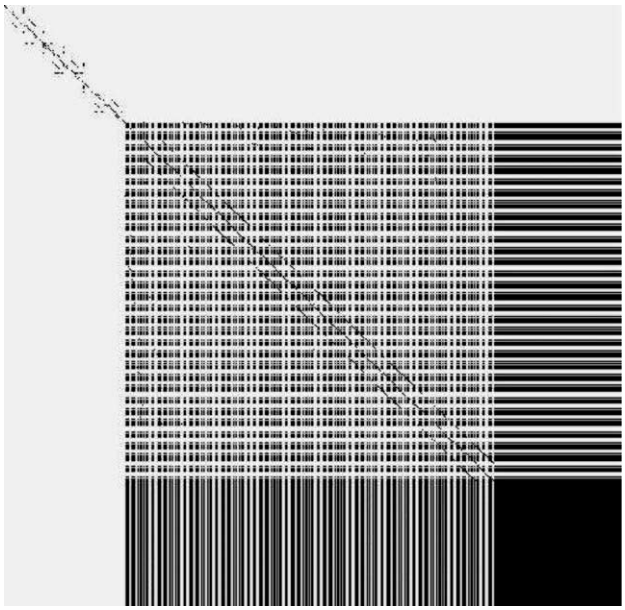

Fig. 12. Sparse pattern for the multi-storey building/raft foundation/ inhomogeneous soil coupling.

Table 6
Time (min) for solution of linear equations with 4431° of freedom and 26% nonzero elements

Methods for solution of linear equations	Pentium III, 1 GHz processor, 1GB PC133 Ram memory	Pentium IV Dual, 1.7 GHz, 2 GB RDRAM
IMSL routines [42]	220	164.1
GMRES [43] ($\varepsilon = 1 \times 10^{-9}$)	46.6	25.4
GMRES [43] ($\varepsilon = 1 \times 10^{-6}$)	22.4	15.2
MA28 [44]	19.0	11.9

8. Conclusion

Inhomogeneous soil-structure interaction was analysed by a BEM–FEM combination. The method of successive stiffness proposed in Ref. [24] was extended to 3D problems, including the influence of the structure's flexibility, using a shell finite element composed of DKT [32] and Free Formulation [33] elements and the results obtained show good agreement with those found in the literature.

Example 7.1 compares analytical and numerical responses. Table 1 presents shows good agreement between both formulations and it also can be seen that the robustness of the responses remained unaltered even when very thin soil layers were considered. The numerical results obtained in example 7.2 demonstrated that the BEM–FEM coupling succeeded well and Table 2 shows the good quality of the displacement and moment values compared with other approaches.

Example 7.3 is concerned with analysing stratified homogeneous soil problems, so the present formulation was compared with the semi-analytical model of [8,9] and Steinbrenner's well-known simplified approach. Results presented in Table 3 demonstrate that the relative displacement errors between [8] and our formulation kept below 1%, where as Steinbrenner's model leads the undeformable layer is near the soil surface [10]. To verify the stability of the present formulation when using several layers to represent the medium, the conventional Mindlin formulation was compared with this work, assuming that all layers have the same physical properties and allowing the thickness of the medium to tend to infinity. The values presented in Table 4 maintained the robustness of the responses and also unaltered when compared with the analytical values.

The purpose of example 7.4 was to check the effects of both the variation of the soil's properties with depth and the position of the undeformable layer on a multi-storey building supported on a raft foundation. The results demonstrated that both these influences are very relevant to a more realistic analysis and design of the building, as can be seen in Figs. 7–11 and Table 5. In this example, the final matrix is sparse and two different known sparse techniques were used. Table 6 showed that it is imperative to apply an appropriate method for this particular kind of matrix, and the free Harwell sparse matrix package demonstrated good efficiency in solving problems based on the mixed BEM–FEM formulation.

Finally, the method of *successive stiffness* offers two computational advantages over the standard boundary element method by zones (subregions), namely: (1) fewer computational operations, and (2) lower storage-memory requirements for equations of the final soil system. It should also be pointed out that the influences of each stratum can be computed independently, so that this technique can be used for distributed-memory computers, with the advantage of achieving high efficiency and loading balance naturally.

Acknowledgements

The authors gratefully acknowledge the financial support of FAPESP (São Paulo State Research Support Foundation, Brazil) for this work.

References

[1] Morris D. Interaction of continuous frames and soil media. J Struct Eng Div ASCE 1966;5:13–43.
[2] Roy R, Dutta SC, Moitra D. Soil–structure interaction in buildings with isolated and grid foundations: a critical study on the state of the art with recommendations. Bridge Struct Eng 2002;31:15–36.
[3] Paiva JB, Butterfield R. Boundary Element analysis of plate–soil interaction. Comput Struct 1997;64:319–28.

[4] Lee IK, Brown PT. Structures–foundation interaction analysis. J Struct Eng Div ASCE 1972;11:2413–31.
[5] Allam MM, Subba RKS, Subramanya IVV. Frame soil interaction and Winkler model, vol. 2. In: Proceedings of Institution of Civil Engineering; 1991. p. 477–94.
[6] Dutta SC, Bhattacharya G, Moitra D. Effect of soil–structure interaction on building frames. Proc Indian Geotech Conf 1999;1: 123–6.
[7] Roy R, Dutta SC. Differential settlement among isolated footings of building frames: the problem, its estimation and possible measures. Int J Appl Mech Eng 2001;6:165–86.
[8] Burmister DM. The general theory of stresses and displacements in layered systems I. J Appl Phys 1945;16:89–96.
[9] Burmister DM. The general theory of stresses and displacements in layered systems III. J Appl Phys 1945;16:296–302.
[10] Poulos HG. Stresses and displacements in an elastic layer underlain by rough rigid base. Géotechnique 1967;17:378–410.
[11] Gibson RE. Some results concerning displacements and stresses in a nonhomogeneous elastic half-space. Géotechnique 1967;17:58–64.
[12] Chan KS, Karasudhi P, Lee SL. Force at a point in the interior of a layered elastic half-space. Int J Solids Struct 1974;10:1179–99.
[13] Ottaviani M. Three-dimensional finite element analysis of vertically loaded pile groups. Géotechnique 1975;25:159–74.
[14] Small JC, Booker JR. Finite layer analysis of layered elastic materials using a flexibility approach, part i-strip loadings. Int J Num Meth Eng 1984;20:1025–37.
[15] Cheung YK, Tham LG, Guo DJ. Analysis of pile group by infinite layer method. Géotechnique 1988;38:415–31.
[16] Booker JR, Carter JP, Small JC. Some recent applications of numerical methods to geotechnical analysis. Comput Struct 1989; 31:81–92.
[17] Romanel C, Kundu T. Soil–structure interaction in a layered medium. Int J Eng Sci 1990;28:191–213.
[18] Lee CY, Small JC. Finite layer analysis of laterally loaded piles in cross-anisotropic soils. Int J Num Meth Geomech 1991;15:785–808.
[19] Chow YK, Teh CI. Pile-cap-pile-group interaction in nonhomogeneous soil. J Geotech Eng 1991;117:1655–68.
[20] Southcott PH, Small JC. Finite layer analysis of vertically loaded piles and pile groups. Comput Geotech 1996;18:47–63.
[21] Ta LD, Small JC. Analysis and performance of piled raft foundations on layered soils-case studies. Soil Foundations 1998;38:145–50.
[22] Banerjee PK. Integral equation methods for analysis of piece-wise nonhomogeneous three-dimensional elastic solids of arbitrary shape. Int J Mech Sci 1976;18:293–303.
[23] Maier G, Novati G. On boundary element-transfer matrix analysis of layered elastic systems. Eng Anal 1986;03(4):208–16.
[24] Maier G, Novati G. Boundary element elastic analysis by a successive stiffness method. Int J Numer Anal Meth Geomech 1987;11:435–47.
[25] Pan E. Static green's functions in multilayered half spaces. Appl Math Modell 1997;21:509–21.
[26] París F, Cañas J. Boundary element method: fundamental and applications. New York: Oxford University Press; 1997.
[27] Hartmann F. Computing the C-matrix in non-smooth boundary points. In: Brebbia CA, editor. New developments in boundary elements methods. Southampton, UK: CMP Publication; 1980.
[28] Love AEH. A treatise on the mathematical theory of elasticity. New York: Dover; 1944.
[29] Brebbia CA, Dominguez J. Boundary elements: an introductory course. Southampton, Boston: Computational Mechanical Publication; 1989.
[30] Aliabadi MH, Hall WS, Phemister TG. Taylor expansions for singular kernels in the boundary element method. Int J Numer Meth Eng 1985; 21:2221–36.
[31] Telles JCF. A self-adaptative co-ordinate transformation for efficient numerical evaluation of general boundary element integrals. Int J Numer Meth Eng 1987;24:959–73.
[32] Bergan PG, Felippa CA. A triangular membrane element with rotational degrees of freedom. Comp Meth Appl Mech Eng 1985;50: 25–69.
[33] Batoz JL, Bathe KJ, Ho LW. A study of three-node triangular plate bending elements. Int J Numer Meth Eng 1980;15:1771–812.
[34] Reddy JN. Energy and variational methods in applied mechanics. New York: Wiley Interscience; 1984.
[35] Fraser RA, Wardle LJ. Numerical analysis of rectangular rafts on layered foundations. Géotechnique 1976;26:613–30.
[36] Sadecka L. A finite/infinite element analysis of thick plate on a layered foundation. Comput Struct 2000;76:603–10.
[37] Wardle LJ, Fraser RA., Finite element analysis of a plate on a layered cross-anisotropic foundation. Proceedings of the First International Conference Finite Element Methods Engineering. University of NSW; 1974.
[38] Kolaî V, Nemec I. Complex automatization of calculations of technical structure interaction problems. Conference of SVTS Kosice; 1983.
[39] Mindlin RD. A force at the interior point of a semi-infinite solid. Physics 1936;7:195–202.
[40] Associação Brasileira de normas Técnicas. Projeto e Execução de Obras de concreto armado-NBR 6118; 2000, in Portuguese.
[41] Associação Brasileira de normas Técnicas. Forças devidas ao vento em edificações-NBR 6123; 1987, in Portuguese.
[42] Aird TJ, Battiste EL, Walton CG. Portability of mathematical software coded in Fortran. ACM Trans Math Software (TOMS) 1977;3(2):113–27.
[43] Youcef S, Schultz MH. GMRES: a generalized minimal residual algorithm for solving nonsymmetric linear systems. SIAM J Sci Stat Comput 1986;7(3):856–69.
[44] Duff IS. MA28—a set of FORTRAN subroutines for sparse unsymmetric linear equations. AERE Report R.8730. London: HMSO; 1977.